

# Electrostatic Regulation of Blue Copper Sites

Daniel Bím,<sup>a</sup> Anastassia N. Alexandrova<sup>\*a,b</sup>

<sup>a</sup>Department of Chemistry and Biochemistry, University of California, Los Angeles, 607 Charles E. Young Drive East, Los Angeles, CA 90095-1569, USA.

<sup>b</sup>California NanoSystems Institute, University of California, Los Angeles, 570 Westwood Plaza, Los Angeles, California 90095-1569, USA.

\*Corresponding author: ana@chem.ucla.edu

---

In the last 50 years, the blue copper proteins became central targets of investigation. Extensive experiments focused on the first- and second-coordination spheres of Cu to probe the effect of local perturbations on its properties. We found that local electric fields, generated by charged residues evolutionarily placed throughout the protein edifice, constitute an additional significant factor regulating blue copper proteins. These fields are not random, but exhibit a highly specific directionality, negative with respect to  $\overrightarrow{\text{Cu-S}_{\text{Cys}}}$  and  $\overrightarrow{\text{Cu-S}_{\text{Met}}}$  in the Cu first shell. The field magnitude contributes to fine-tuning of the geometric and electronic properties of Cu sites in individual blue copper proteins. Specifically, the local electric fields evidently control the Cu-S<sub>Met</sub> bond distance, Cu(II)-S<sub>Cys</sub> bond covalency, and the energies of the frontier molecular orbitals, which, in turn, govern the Cu(II/I) reduction potential and the relative absorption intensities at 450 nm and 600 nm.

---

## Introduction

Blue copper proteins (BC; also type 1 or T1 proteins) are proteins that participate in the rapid long-range biological electron transfers.<sup>1–4</sup> Their Cu(II) centers feature an intense 600-nm band in the electronic absorption spectra, giving rise to their blue color and their name. A typical BC active site (e.g., in plastocyanin, azurin, rusticyanin, amicyanin) consists of the Cu(II) coordinated by 2His, Cys, and Met ligands in the pseudotetrahedral geometry.<sup>5,6</sup> Since the preferred coordination of Cu(II) complexes is square planar,<sup>4</sup> it was initially thought that observed tetrahedral geometry is responsible for their distinct spectral features, including small EPR hyperfine splitting, and high Cu(II/I) reduction potentials.<sup>7–15</sup> Additionally, the unusual coordination, along with relatively small geometric changes between oxidized and reduced states (e.g., small angular distortion, small differences in Cu-L bond lengths, and rigidity of proteins upon single-point mutations),<sup>16–22</sup> laid the foundations of entatic<sup>23</sup> and rack-induced<sup>24</sup> concepts in bioinorganic chemistry. According to the entatic/rack hypothesis, the protein function (e.g., electron transfer) is empowered by keeping the active site in a distorted (compromised) structure between the two functional states; such as Cu(I) (tetrahedral) and Cu(II) (square planar) conformations in BC proteins. Hence, the reorganization energy of redox reaction is minimized,<sup>4,25</sup> and following the Marcus theory,<sup>26</sup> the rate of electron transfer is enhanced. Note that electron-transfer proteins must operate near thermodynamic neutrality, making the argument of small reorganization energy critical for their proper biological function.<sup>4</sup>

However, the entatic/rack concepts were questioned both in computations and in spectroscopic studies.<sup>19,27</sup> Solomon and co-workers demonstrated that tetrahedral structure is indeed preferred in Cu(II) BC proteins; however, not due to entatic/rack constraints of Cu(II) coordination geometry in a true sense but rather due to the Cu-S<sub>Met</sub> bond elongation and Cu-S<sub>Cys</sub> bond shortening in the Cu first ligand shell.<sup>19</sup> Such distortions in Cu ligand field lowers the site's symmetry (i.e., orbital degeneracy)

and eliminates the Jahn-Teller distorting forces otherwise present in tetrahedral Cu(II) complexes.<sup>28</sup> The abnormally elongated axial Cu-S<sub>Met</sub> and shortened equatorial Cu-S<sub>Cys</sub> bonds are unique, and likely controlled by the constraints produced by the protein.<sup>29–31</sup>

It was recognized that Cu-S<sub>Met</sub> and Cu-S<sub>Cys</sub> bonds are electronically and geometrically coupled,<sup>2,12,19,32</sup> so that the weak Cu-S<sub>Met</sub> interaction is compensated by strengthening Cu-S<sub>Cys</sub>, together with increasing the Cu(II)-S<sub>Cys</sub> bond covalency.<sup>4,33</sup> In turn, strong Cu-S<sub>Cys</sub> is accountable for a strong electronic absorption at 600 nm due to S<sub>Cys</sub> 3p → Cu(II) 3d<sub>x<sub>2</sub>-y<sub>2</sub></sub> π charge transfer.<sup>34–36</sup> The high covalency of Cu(II) 3d<sub>x<sub>2</sub>-y<sub>2</sub></sub> HOMO also results in a small EPR hyperfine splitting.<sup>35</sup> By regulating the strengths of the Cu-S<sub>Met</sub> and Cu-S<sub>Cys</sub> bonds, the BC proteins might thus tune their properties toward desired functionalities, including adjustment of Cu(II/I) reduction potential or rate of electron transfer.<sup>31,35,37,38</sup> However, the mechanism of such regulation remains debated.

Within the Cu(I) sites in the BC proteins, Solomon has argued that Met ligand is held in place by the protein environment – i.e., in the entatic or rack-induced state.<sup>39</sup> However, a discussion is complicated by the fact that there is not an unambiguous definition of what entasis is and/or how strain energy in the metal site should be quantified.<sup>27,40,41</sup> As an example, Ryde et al. contrariwise proposed that BC proteins *are not* entatic.<sup>27</sup> Instead, the Met residue was foreseen to be selected as a ‘floppy’ ligand with a flat potential energy surface to accommodate facile interchange between the two oxidation states and assist with rapid electron transfer. On the other hand, Hurd et al.<sup>42</sup> computed much higher strain energies for plastocyanin when they included not only geometric constraints (i.e., covalent strain) but also protein electrostatics from QM/MM calculations. The strain energies elevated by ~10 kcal mol<sup>-1</sup>. In plastocyanin, this suggests that protein electrostatics may play a significant role in Cu-S<sub>Met</sub>/Cu-S<sub>Cys</sub> regulation and can contribute to plastocyanin function. Electrostatic interactions were also evidenced as predominant determinants of Cu(II/I)

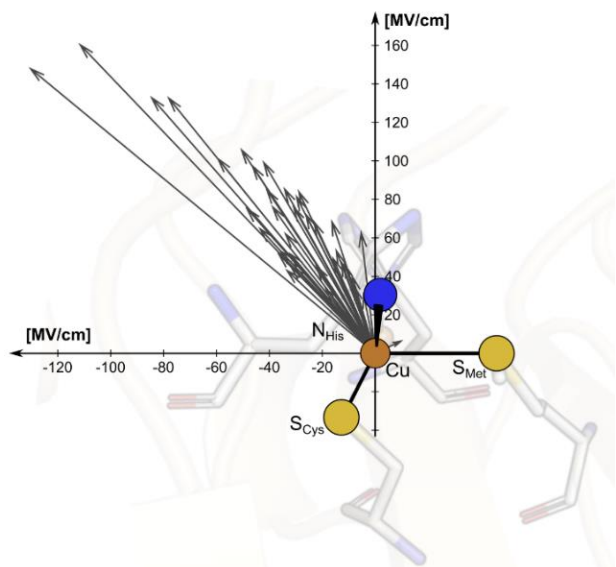


**Figure 2.** A graphical representation of the LEFs found in the series of BC proteins. The LEFs are plotted with gray arrows as vectors projected in the  $\text{Cu-S}_{\text{Cys}}/\text{Cu-S}_{\text{Met}}$  plane.

reduction potentials in the computational study of BC azurin variants.<sup>43</sup>

Recently, we have demonstrated that heme-iron proteins exert highly specific intramolecular electric fields on their active sites and that there is a strong correlation between the direction and magnitude of this field and the protein function.<sup>44</sup> Herein, we demonstrate that the local electric fields produced by the proteins of the BC family are likewise not randomly oriented and instead appear customized by the evolution to fine-tune the BC centers' properties. This includes modifying the BC site geometry, electronic structure, BC spectral features, and  $\text{Cu(II/I)}$  reduction potentials.

## Results and Discussion

### The local electric fields in the active sites of blue copper proteins.

Employing the Erebus PDB protein substructure search server,<sup>45</sup> we have identified 36 unique BC proteins with 2His, Cys, Met coordination (see Computational Details section in the SI). For this set of proteins, we analyzed the magnitudes of local electric fields (LEFs) in their active sites' Cu, together with the geometrical features of the proteins' active sites from their crystal structures (Table S1). Note that the evaluated fields are induced by the entire protein outside of the BC active site, i.e., excluding the effects of coordinating residues and the Cu itself. The coordinating ligands thus do not contribute to the discussed LEFs, and the effect of LEFs is thereby additive to the effect of the first coordination sphere on the metal.

The overall LEF magnitudes range significantly in the protein series, from  $14 \text{ MV cm}^{-1}$  (1a3z; rusticyanin) to  $165 \text{ MV cm}^{-1}$  (1e2z;

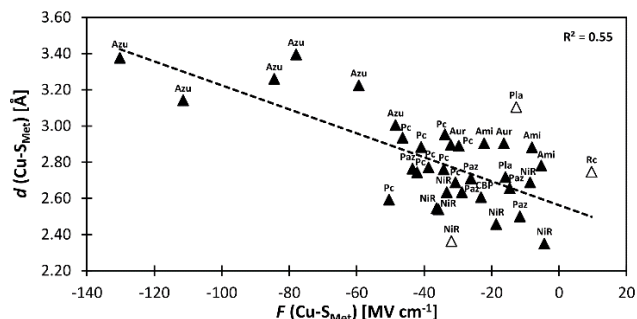


**Figure 1.** A correlation between  $\text{Cu-S}_{\text{Met}}$  bond distances ( $d(\text{Cu-S}_{\text{Met}})$ ) and projections of the LEF vector in the  $(\text{Cu-S}_{\text{Met}})$  orientation ( $F(\text{Cu-S}_{\text{Met}})$ ) for the BC proteins from Table S1. The empty triangles represent proteins that were crystallized in the reduced form and are excluded from the fit. Ami = amicyanin, Aur = auracyanin, Azu = azurin, CBP = cucumber basic protein, Nir = nitrite reductase, Pla = plantacyanin, Pc = plastocyanin, Paz = pseudoazurin, Rc = rusticyanin.

C3A/C26A azurin mutant). However, the LEFs are not randomly oriented (Figure 1). Instead, the LEFs projected in the  $\text{Cu-S}_{\text{Met}}$  and  $\text{Cu-S}_{\text{Cys}}$  directions are preferentially negative (cf. average  $F(\text{Cu-S}_{\text{Met}}) = -35.5 \text{ MV cm}^{-1}$  and  $F(\text{Cu-S}_{\text{Cys}}) = -47.4 \text{ MV cm}^{-1}$ ), and the average LEFs projected in the  $\text{Cu-N}_{\text{His}}$  directions are preferentially positive (average  $F(\text{Cu-N}_{\text{His}}) = +36.4 \text{ MV cm}^{-1}$ ).

We indeed found a passable correlation between the computed  $F(\text{Cu-S}_{\text{Met}})$  projection on this bond and the  $\text{Cu-S}_{\text{Met}}$  distance ( $d(\text{Cu-S}_{\text{Met}})$ ) (Figure 2). This is consistent with a facile electrostatic regulation of the  $\text{Cu-S}_{\text{Met}}$  bond due to a very flat potential energy surface along this coordinate. However, since a significantly worse correlations were found between LEF (or its projections) and other BC geometric features – such as  $d(\text{Cu-S}_{\text{Cys}})$  or  $d(\text{Cu-S}_{\text{Cys}})/d(\text{Cu-S}_{\text{Met}})$  ratio, or the  $\tau$  angle<sup>‡</sup> (Figures S1-S4) – it appears that translation to BC site geometry or their spectral properties might be more intricate. As an example, Szuster et al. demonstrated that other factors, e.g., Cu ligand-loop hydrophobicity or water accessibility of the Cu site, also influence the active site geometry, and the  $\text{Cu(II/I)}$  reduction potentials and electronic absorption intensities in the  $\text{Cu}_A$ -based copper sites.<sup>46</sup>

### Coupled nature of the $\text{Cu-S}_{\text{Met}}$ and $\text{Cu-S}_{\text{Cys}}$ bonds.

To evaluate how the change of  $d(\text{Cu-S}_{\text{Met}})$  in the BC site influences  $d(\text{Cu-S}_{\text{Cys}})$ , we have performed a constrained two-dimensional potential energy surface scan in the cluster model of the oxidized poplar plastocyanin (PDB code: 4dp9) coordination geometry (Figure 3, top left).<sup>5</sup> The equilibrium structure is found at the  $d(\text{Cu-S}_{\text{Met}}) = 2.50 \text{ \AA}$  and  $d(\text{Cu-S}_{\text{Cys}}) = 2.20 \text{ \AA}$ . This is slightly distorted from the oxidized plastocyanin crystal-structure geometry ( $d(\text{Cu-S}_{\text{Met}}) = 2.78 \text{ \AA}$  and  $d(\text{Cu-S}_{\text{Cys}}) = 2.16 \text{ \AA}$ );<sup>47</sup> however, the energy difference is only  $\sim 1.8 \text{ kcal mol}^{-1}$ . Consistent with Ryde's results (based on the cluster-model approach without protein electrostatics),<sup>27</sup> we show that  $\text{Cu-S}_{\text{Met}}$  bond is considerably more flexible, with an enthalpic

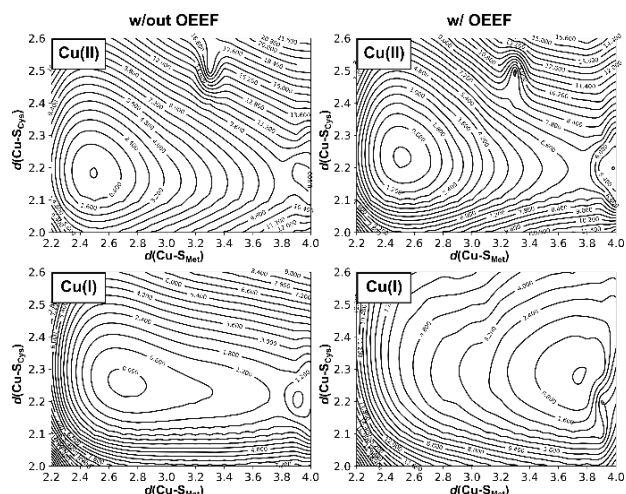


**Figure 3.** The effect of the protein LEF on the two-dimensional potential energy surfaces correlating the  $d(\text{Cu-S}_{\text{Cys}})$  and  $d(\text{Cu-S}_{\text{Met}})$  bond distances. Graphs for Cu(II) and Cu(I) (*top* and *bottom*) oxidation states are shown; without the applied external electric field (*left*) and with applied external electric field (corresponding to the average LEF found in the series of BC proteins; *right*). The potential energies are plotted in  $\text{kcal mol}^{-1}$  as iso-contour lines and are referenced to the lowest-energy point in each graph.

penalty of only ca.  $0.3 \text{ kcal mol}^{-1}$ , associated with displacement of  $\sim 0.1 \text{ \AA}$  from the equilibrium geometry. On the other hand, the same displacement of the Cu-S<sub>Cys</sub> bond costs ca.  $1.0 \text{ kcal mol}^{-1}$  in enthalpy. In the Cu(I) oxidation state, the lowest-energy structure has the Cu-S<sub>Met</sub> bond stretched to  $2.70 \text{ \AA}$  and is ca.  $0.5 \text{ kcal mol}^{-1}$  below the geometry with  $d(\text{Cu-S}_{\text{Met}}) = 2.50 \text{ \AA}$  preferred in Cu(II) (Figure 3, *bottom left*). However, the potential energy surface is yet shallower in the direction toward Cu-S<sub>Met</sub> dissociation, with a barrier of only  $\sim 2 \text{ kcal mol}^{-1}$  between the two minima with the associated and dissociated Met ligand.

Application of oriented external electric field (OEEF) in the average BC site orientation and magnitude (*cf.* Figure 1) leads to almost no change in the preferred Cu(II) geometry or potential energy surface (Figure 3, *top right*). However, despite small geometric differences, we note that OEEF remarkably reduces the HOMO/LUMO gap between the frontier molecular orbitals (Cu(II)  $\alpha$  HOMO and Cu(II)  $\beta$  LUMO) by  $28 \text{ kcal mol}^{-1}$  and Cu(II)-S<sub>Cys</sub> bond covalency by  $\sim 24 \%$  – as indicated by the change in Cu and S<sub>Cys</sub> spin densities in the Cu(II) equilibrium structure (the calculated spin densities are: Cu = 0.34, S<sub>Cys</sub> = 0.51 at  $F = 0$  and Cu = 0.49, S<sub>Cys</sub> = 0.27 at average  $F$  experienced by any BC site) (*cf.* Table 1). In contrast, there is no stable structure with bonded Met when the OEEF is applied to the Cu(I) site. Instead, the Met ligand dissociates to  $d(\text{Cu-S}_{\text{Met}}) = 3.90 \text{ \AA}$ . This suggests that, although the enzyme geometry would be enthalpically favored in Cu(I) oxidation state without LEF, in the average BC site (with the LEF opposing  $\overrightarrow{\text{Cu-S}_{\text{Met}}}$ ) the Cu-S<sub>Met</sub> bond must be covalently constrained by the protein, in order to compensate both the enthalpic and the entropic penalties. Herein, the average LEF was found to introduce an enthalpic strain of  $\sim 4 \text{ kcal mol}^{-1}$  compared to an unconstrained geometry. We suggest

**Table 1.** Calculated Cu(II)  $\alpha$  HOMO and Cu(II)  $\beta$  LUMO energies and the Mulliken spin densities of the selected atoms (at the B3LYP/def2-TZVP level) for the equilibrium structure from Figure 3.

Orbital energy [eV]	w/out OEEF	w/ OEEF
Cu(II) $\alpha$ HOMO	-7.21	-6.50
Cu(II) $\beta$ LUMO	-4.75	-5.25
Mulliken spin density [e]	w/out OEEF	w/ OEEF
Cu	0.34	0.49
S <sub>Cys</sub>	0.51	0.27
S <sub>Met</sub>	0.08	0.05
N <sub>His</sub> <sup>[a]</sup>	0.06	0.17

[a] Combined spin density on both coordinating N<sub>His</sub> atoms.

the enthalpic penalty should be added to an entropic penalty of  $\sim 4.5 \text{ kcal mol}^{-1}$  proposed by Solomon,<sup>35</sup> leading to the total strain energy of  $\sim 8.5 \text{ kcal mol}^{-1}$  that is associated with constraining the Met ligand in an average Cu(I) BC site.

#### Effect of the local electric field on the blue copper properties.

Although there is no significant geometrical change in the Cu(II) BC site under OEEF, the quantum chemical calculations revealed that frontier molecular orbitals are substantially altered in energy, along with a decrease of the Cu(II)-S<sub>Cys</sub> bond covalency by  $\sim 24 \%$ . A lower covalency is quantified by the lower Mulliken spin density at the S<sub>Cys</sub> atom, indicating smaller S<sub>Cys</sub> 3p and Cu 3d<sub>x<sup>2</sup>-y<sup>2</sup></sub> orbitals overlap and hence bonding (Table 1).<sup>35</sup> Similarly, smaller bonding in Cu(II)  $\alpha$  HOMO can be translated into lower antibonding character in Cu(II)  $\beta$  LUMO, which is exhibited by a significantly decreased Cu(II)  $\beta$  LUMO energy under OEEF, by  $\sim 11.5 \text{ kcal mol}^{-1}$ . By evaluating the individual contributions from  $F(\text{Cu-S}_{\text{Cys}})$  and  $F(\text{Cu-S}_{\text{Met}})$  projections of the LEF (*cf.* Table S2, where we applied OEEF only in the  $\overrightarrow{\text{Cu-S}_{\text{Cys}}}$  or  $\overrightarrow{\text{Cu-S}_{\text{Met}}}$  direction), we can conclude that the decreased Cu(II)-S<sub>Cys</sub> bond covalency and Cu(II)  $\beta$  LUMO energy are caused by  $F(\text{Cu-S}_{\text{Cys}})$  projection of the LEF, which exhibits decreased S<sub>Cys</sub> spin density by  $0.21 e$  and Cu(II)  $\beta$  LUMO energy by  $7.7 \text{ kcal mol}^{-1}$ . On the other hand, the average OEEF in  $\overrightarrow{\text{Cu-S}_{\text{Met}}}$  projection increases the Cu(II)-S<sub>Cys</sub> bond covalency by  $\sim 6 \%$  with Cu(II)  $\beta$  LUMO decrease by only  $0.7 \text{ kcal mol}^{-1}$ . Note that the projections are not orthogonal and their effects thus cannot be fully decoupled.

Many BC features were previously correlated with the Cu(II)-S<sub>Cys</sub> bond covalency, and our results therefore suggest that LEF may play a critical role in tuning the BC properties. For instance, the BC proteins' electronic absorption spectra are characterized by the distinctive absorption bands at  $\sim 600 \text{ nm}$  and  $\sim 450 \text{ nm}$ . The BC proteins have stronger absorption intensity at the lower-energy thiolate  $\pi$ -to-Cu charge-transfer transition and weaker absorption intensity at the higher-energy  $\sigma$ -to-Cu charge-transfer transition (Figure 4). Inversely, the  $\epsilon_{600}$  and  $\epsilon_{450}$

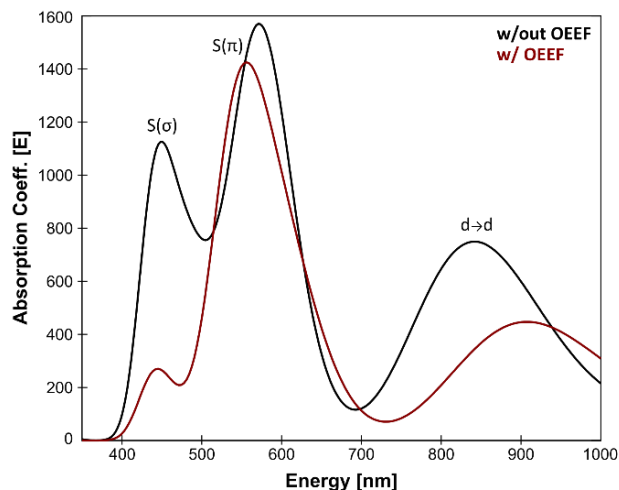


**Figure 4.** Calculated TD-DFT spectra for the equilibrium structure from **Figure 3**; without the applied external electric field (*black*) and with applied external electric field (corresponding to the average LEF found in the series of BC proteins; *red*). A lower Cu(II)-S<sub>Cys</sub> bond covalency under applied OEEF is translated into a considerably smaller  $\sigma$ -to-Cu charge-transfer transition at  $\sim 450$  nm.

intensities are reversed for the normal tetragonal cupric complexes and green copper proteins. A lower Cu(II)-S<sub>Cys</sub> bond covalency in our computational model due to lower  $F(\text{Cu-S}_{\text{Cys}})$  is thus consistent with a shift toward a more pronounced blue copper absorption features (*cf.* **Figure 4**). Hence, the  $\epsilon_{450}/\epsilon_{600}$  ratio is  $\sim 0.7$  for the equilibrium Cu(II) geometry from **Figure 3** without the applied field, while the  $\sigma$ -to-Cu charge-transfer intensity is significantly diminished by the OEEF, leading to an  $\epsilon_{450}/\epsilon_{600}$  ratio of  $\sim 0.2$ . Significantly, the  $\epsilon_{450}/\epsilon_{600}$  ratio is regularly utilized as a measure of the cupric coordination geometry.<sup>2</sup> Its sensitivity to the local intramolecular electric field exerted on the Cu site is striking.

The effect of  $F(\text{Cu-S}_{\text{Cys}})$  on the electronic absorption spectra is further reflected for blue copper and green copper proteins in **Table S1**. While the average  $F(\text{Cu-S}_{\text{Cys}})$  is  $-26.7$  MV cm<sup>-1</sup> for nitrite reductases (green copper proteins), the remaining proteins exhibit  $F(\text{Cu-S}_{\text{Cys}})$  of  $-52.3$  MV cm<sup>-1</sup> (i.e.,  $\sim 25$  MV cm<sup>-1</sup> lower). We also note that  $F(\text{Cu-S}_{\text{Met}})$  projection of the LEF is as well higher for nitrite reductases by  $\sim 15$  MV cm<sup>-1</sup>, which is consistent with a shorter  $d(\text{Cu-S}_{\text{Met}})$  witnessed in green copper proteins (*cf.* correlation of  $d(\text{Cu-S}_{\text{Met}})$  vs.  $F(\text{Cu-S}_{\text{Met}})$  for nitrite reductases in **Figure 2**).

As for the effect of LEF on the Cu(II/I) reduction potential, a lower Cu(II)-S<sub>Cys</sub> covalency indicates a weaker Cu-S<sub>Cys</sub> bond, which agrees with a destabilization of the oxidized Cu(II) state and thus higher Cu(II/I) reduction potential. According to Hadt et al., the Cu(I) adiabatic ionization energy (i.e., the inverse of the Cu(II) adiabatic electron affinity) is decreased due to lowered Cu(II)-S<sub>Cys</sub> covalency by  $\sim 10$  mV per 1% decrease of the spin density on S<sub>Cys</sub>.<sup>48</sup> Therefore, on average, we might assign the effect of  $\sim 240$  mV increase in the Cu(II) electron affinity due

to lowered Cu(II)-S<sub>Cys</sub> covalency in an average BC. Similarly, when the average OEEF is applied, the redox-active molecular orbital (i.e., Cu(II)  $\beta$  LUMO) is decreased in energy by ca. 11.5 kcal mol<sup>-1</sup> (*cf.* **Table 1**), consistent with an increase in the Cu(II) electron affinity by ca. 500 mV (i.e., the effect that is twice as high as for the Cu(II) electron affinity predicted from a decreased covalency). With simplification, we can thus attribute the increase in the Cu(II) electron affinity to a comparable covalent and non-local electrostatic contributions to the Cu(II)  $\beta$  LUMO energy.

Finally, note that  $F(\text{Cu-S}_{\text{Cys}})$  and  $F(\text{Cu-S}_{\text{Met}})$  contribute to the overall Cu(II/I) reduction potential in the same direction. Although a negative  $F(\text{Cu-S}_{\text{Met}})$  leads to a higher Cu(II)-S<sub>Cys</sub> covalency by  $\sim 6\%$  (decreasing the Cu(II) electron affinity by  $\sim 60$  mV), there is a significant antagonistic contribution of  $F(\text{Cu-S}_{\text{Met}})$  to the Cu(I) strain energy, increasing the Cu(II/I) reduction potential by  $\sim 170$  mV (*vide supra*). All in all, the average LEF in BC proteins appears to increase the Cu(II/I) reduction potential on aggregate by ca. 670 mV, coming from the increased Cu(II)-S<sub>Cys</sub> covalency (240 mV), non-local electrostatic contributions to the Cu(II)  $\beta$  LUMO energy (260 mV), and increased Cu(I) strain energy (170 mV).

#### Electrostatic contribution to the azurin Cu(II/I) reduction potentials.

To further support the idea of LEF regulating the BC sites' electronic structure, including Cu(II/I) reduction potentials, we have calculated the LEFs in a series of azurin variants from ref. 49. Specifically, we have analyzed all of the variants not containing mutations in the Cu first shell<sup>55</sup> (i.e., N47S, F114N, F114P, and N47S/F114N), which were generated from the available PDB structures of the wild-type azurin (4azu), and N47S/F114N (3jtb) and F114P/M121Q (3in0) azurin variants.

As compared to wild-type azurin, the N47S, F114N, and N47S/F114N have higher Cu(II/I) reduction potentials, which are consistent with their lower (more negative)  $F(\text{Cu-S}_{\text{Cys}})$  projections of the LEF (**Figure 5A**). Oppositely, a higher  $F(\text{Cu-S}_{\text{Cys}})$  of the F114P variant agrees remarkably well with lower Cu(II/I) reduction potential. Since the regression coefficient ( $R^2$ ) in **Figure 5A** is close to unity, we can estimate an increase in reduction potential due to  $F(\text{Cu-S}_{\text{Cys}})$  as  $-12.5$  mV / 1 MV cm<sup>-1</sup>. This also agrees well with the computational model presented above correlating the OEEF with the Cu(II)  $\beta$  LUMO energy and Cu(I) strain energy contributions to the Cu(II/I) reduction potentials (i.e.,  $-670$  mV / 47.4 MV cm<sup>-1</sup> =  $-14.1$  mV / 1 MV cm<sup>-1</sup>). We note in passing that  $F(\text{Cu-S}_{\text{Cys}})$  projection of the LEF in the azurin variants also weakly correlates with the experimentally determined Cu(II)-S<sub>Cys</sub> bond covalencies: 54 % for F114P, 45 % for wild-type azurin, 43 % for F114N, and 31 % for N47S.<sup>48</sup>

An excellent correlation in **Figure 5A** suggests that determinants of the reduction potentials in the azurin variants are purely electrostatic. However, this study benefits from using

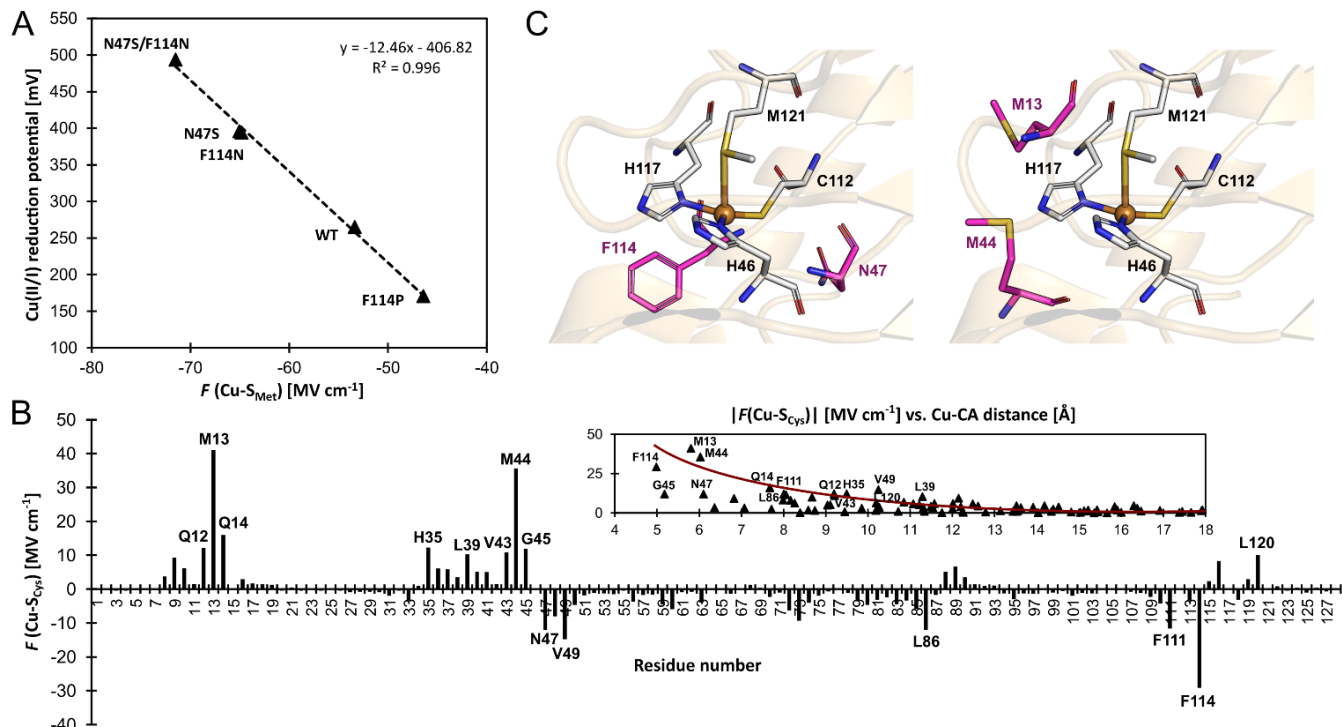


**Figure 5.** A: Correlation between experimental one-electron Cu(II/I) reduction potentials (referenced to normal hydrogen electrode) vs.  $F(\text{Cu-S}_{\text{Cys}})$  projection of the LEF in a series of azurin variants from ref. [49]. B: A contribution of each residue's side chain toward  $F(\text{Cu-S}_{\text{Cys}})$  in the wild-type azurin. Note that side chains of the ligating (first-shell) residues are not included. A more significant contribution to  $F(\text{Cu-S}_{\text{Cys}})$  is from the residues closer to the Cu site; the contribution becomes negligible when Cu- $\text{C}_\alpha$  distance exceeds  $\sim 15$  Å. C: The second-coordination shell residues subjected to mutation to alter azurin Cu(II/I) reduction potential (in purple) investigated in ref. [49] (*left*) and suggested in this work (*right*).

the crystal structures, which already reflect the effect of the field. For example, the crystal structure of the F114P variant is missing an important Cys...HN- $\text{C}_\alpha$ -CO hydrogen bond. However, if the F114P mutant is modeled by a simple amino acid replacement in the wild-type azurin, a non-equilibrated structure with that hydrogen bond is yielded, and a much lower  $F(\text{Cu-S}_{\text{Cys}})$  by  $\sim 14$  MV  $\text{cm}^{-1}$  is predicted, which significantly deviates from the fit. The crystal structure or a structure produced by extensive molecular dynamics equilibration is needed for accurate predictions. Still, the correlation between the change of the reduction potential and the local electric field calculated directly from the crystal structure represents a powerful and economic concept that can be utilized, e.g., for designing BC variants with specific redox properties.

In this regard, we have analyzed the contributions of individual residues in the wild-type azurin (4azu) toward the observed  $F(\text{Cu-S}_{\text{Cys}})$  (see **Note S2** in the SI for details); the effect of the residues' side chains is presented in **Figure 5B** (the overall effect of each residue and the backbone-only contributions are shown in **Figure S6**). Not surprisingly, the electric field beyond the first-coordination sphere is mainly dictated by the side chains of the second sphere residues, and the effect on the  $F(\text{Cu-S}_{\text{Cys}})$  drops significantly with the increasing distance of a residue from Cu (*cf.* **Figure 5B** and **Figure S7**). However, some impactful residues in the second sphere have not been

experimentally examined. Especially, we hypothesize that 13M and 44M on the opposite side of the first-shell 112C generate substantial dipole moments that should influence the azurin redox properties considerably (**Figure 5B-C**). By removing both of the dipoles via mutating the Met residues, we propose that it should be possible to lower  $F(\text{Cu-S}_{\text{Cys}})$  by as much as 80 MV  $\text{cm}^{-1}$ , and thus increase the reduction potential roughly by  $\sim 1$  V (evaluation of the protein structure upon mutation is required for a more accurate prediction).

## Conclusions

By examining an extensive series of blue copper proteins' crystal structures, we show that the protein scaffolds that host blue copper sites are not mere spectators of their function. Instead, the proteins' local electric fields can regulate multiple geometric and electronic properties typical of blue copper sites in biology. Specifically, we demonstrate that the local electric fields are oriented in a definite way throughout the blue copper protein family to modulate the copper interactions with its ligating residues. By orienting the electric field preferentially in the direction opposite of the  $\overrightarrow{\text{Cu-S}_{\text{Cys}}}$  and  $\overrightarrow{\text{Cu-S}_{\text{Met}}}$  vectors in the copper first shell, the proteins make the Cu-S bonds considerably weaker than those in the isolated blue copper sites in a vacuum.

In the context of entatic/rack-induced concepts, the  $F(\text{Cu-S}_{\text{Met}})$  projection of the field pushes the axial Met ligand to dissociate from the Cu(I) center, though the entities are still held together by the protein. Hence, the electric field can be seen as an additional element adding to the Cu(I) sites' covalent strain. In an average blue copper site, we have estimated an enthalpic destabilization of the constrained Cu(I) active site by  $\sim 4$  kcal mol<sup>-1</sup> due to local electric field.

Importantly, a weakening of the Cu-S<sub>Cys</sub> bond appears to considerably influence many blue copper spectroscopic properties. Besides others, a weaker Cu-S<sub>Cys</sub> is consistent with decreasing the Cu(II)-S<sub>Cys</sub> bond covalency, which, in turn, affects the relative absorption intensities of Cu(II) at 450 nm and 600 nm. We have demonstrated that, while the  $\epsilon_{450}/\epsilon_{600}$  ratio is  $\sim 0.7$  for the isolated equilibrium Cu(II) geometry in the plastocyanin active site, the local electric field oriented in the direction opposite of  $\overrightarrow{\text{Cu-S}_{\text{Cys}}}$  (average projection of  $F(\text{Cu-S}_{\text{Cys}})$  is  $-47.4$  MV cm<sup>-1</sup>) is necessary to shift the  $\epsilon_{450}/\epsilon_{600}$  to  $\sim 0.2$ , consistent with that of the regular blue copper sites. On the contrary, the green copper proteins exhibit much lower magnitudes of the local electric fields (average  $F(\text{Cu-S}_{\text{Cys}})$  is  $-26.7$  MV cm<sup>-1</sup>), in accordance with their higher  $\epsilon_{450}/\epsilon_{600}$  ratio.

The electric field also contributes to the high Cu(II/I) reduction potentials of the blue copper sites. On average, it was found to be accountable for an increase of the Cu(II/I) reduction potentials by ca. 670 mV, originating from a lower Cu(II)-S<sub>Cys</sub> covalency (240 mV), non-local contributions to a lower Cu(II)  $\beta$  LUMO energy (260 mV), and increased Cu(I) strain energy (170 mV).

Last but not least, we have observed that local electric field is a critical determinant of the Cu(II/I) reduction potentials, when comparing different variants of otherwise identical blue copper sites. In a series of azurin variants that introduced mutations in the second-coordination sphere of the Cu site, we have shown that the change of reduction potential can be accurately described by the change in the local electric field exerted on the Cu-S<sub>Cys</sub> bond in the equilibrium structure. We suggest that this concept could be utilized for designing protein variants with desired redox properties. Following our analysis, we propose new targets for mutagenetic studies, which have not been questioned thus far, and which contribute significantly to  $F(\text{Cu-S}_{\text{Cys}})$  and should alter the reduction potential.

## Acknowledgements

Financial support comes from the NIH 1R01GM134047 grant to A.N.A.. We also acknowledge the UCLA-IDRE cluster Hoffman2 and XSEDE for computational resources.

## Notes and references

- ‡  $\tau = (360^\circ - (\alpha + \beta)) / (141^\circ)$ , where  $\alpha$  and  $\beta$  are the two largest angles between the Cu ligating atoms. The parameter  $\tau$  was introduced by Yang et al.<sup>50</sup> as a four-coordinate geometry index ranging from perfect tetrahedral ( $\tau = 1$ ) to perfect square planar ( $\tau = 0$ ).
- § In the two-dimensional scan, we incrementally altered the Cu-S<sub>Cys</sub> and Cu-S<sub>Met</sub> distances by 0.1 Å, while keeping the rest of the coordination geometry (i.e., angles between Cu ligating atoms ( $\tau$ ), and Cu-N<sub>His</sub> distances) at the crystal positions. See Computational Details section in the SI.
- §§ In our approach, the LEF is analyzed outside the first-shell sphere of ligands (i.e., charges of the side-chains of ligating residues are zeroed). Therefore, any mutations in the Cu first shell would not result in different LEFs.
- 1 J. Liu, S. Chakraborty, P. Hosseinzadeh, Y. Yu, S. Tian, I. Petrik, A. Bhagi and Y. Lu, *Chem. Rev.*, 2014, **114**, 4366–4469.
  - 2 E. I. Solomon and R. G. Hadt, *Coord. Chem. Rev.*, 2011, **255**, 774–789.
  - 3 E. I. Solomon, R. K. Szilagy, S. DeBeer George and L. Basumallick, *Chem. Rev.*, 2004, **104**, 419–458.
  - 4 H. B. Gray, B. G. Malmström and R. J. P. Williams, *JBC J. Biol. Inorg. Chem.*, 2000, **5**, 551–559.
  - 5 E. I. Solomon, J. W. Hare and H. B. Gray, *Proc. Natl. Acad. Sci.*, 1976, **73**, 1389–1393.
  - 6 J. M. Guss and H. C. Freeman, *J. Mol. Biol.*, 1983, **169**, 521–563.
  - 7 L. Broman, B. G. Malmström, R. Aasa and T. Vänngård, *Biochim. Biophys. Acta*, 1963, **75**, 365–376.
  - 8 E. I. Solomon, M. J. Baldwin and M. D. Lowery, *Chem. Rev.*, 1992, **92**, 521–542.
  - 9 E. I. Solomon and M. D. Lowery, *Science (80- )*, 1993, **259**, 1575–1581.
  - 10 E. I. Solomon, K. W. Penfield and D. E. Wilcox, in *Copper, Molybdenum, and Vanadium in Biological Systems*, eds. B. A. Averill, L. R. Briggs, N. D. Chasteen, T. R. Gilbert, K. Kustin, G. C. McLeod, K. W. Penfield, E. I. Solomon and D. E. Wilcox, Springer Berlin Heidelberg, Berlin, Heidelberg, 1983, pp. 1–57.
  - 11 D. W. Randall, S. D. George, B. Hedman, K. O. Hodgson, K. Fujisawa and E. I. Solomon, *J. Am. Chem. Soc.*, 2000, **122**, 11620–11631.
  - 12 L. B. LaCroix, S. E. Shadle, Y. Wang, B. A. Averill, B. Hedman, K. O. Hodgson and E. I. Solomon, *J. Am. Chem. Soc.*, 1996, **118**, 7755–7768.
  - 13 R. J. P. Williams, *Inorganica Chim. Acta Rev.*, 1971, **5**, 137–155.
  - 14 R. Malkin and B. G. Malmström, *Adv. Enzymol. Relat. Areas Mol. Biol.*, 1970, 177–244.
  - 15 B. G. Malmström, B. Reinhammar and T. Vänngård, *Biochim. Biophys. Acta - Bioenerg.*, 1970, **205**, 48–57.
  - 16 A. L. Le Sueur, R. N. Schauggaard, M.-H. Baik and M. C. Thielges, *J. Am. Chem. Soc.*, 2016, **138**, 7187–7193.
  - 17 J. M. Guss, H. D. Bartunik and H. C. Freeman, *Acta Crystallogr. Sect. B*, 1992, **48**, 790–811.

- 18 J. M. Guss, P. R. Harrowell, M. Murata, V. A. Norris and H. C. Freeman, *J. Mol. Biol.*, 1986, **192**, 361–387.
- 19 J. A. Guckert, M. D. Lowery and E. I. Solomon, *J. Am. Chem. Soc.*, 1995, **117**, 2817–2844.
- 20 W. E. B. Shepard, B. F. Anderson, D. A. Lewandoski, G. E. Norris and E. N. Baker, *J. Am. Chem. Soc.*, 1990, **112**, 7817–7819.
- 21 A. Romero, C. W. G. Hoitink, H. Nar, R. Huber, A. Messerschmidt and G. W. Canters, *J. Mol. Biol.*, 1993, **229**, 1007–1021.
- 22 B. G. Karlsson, R. Aasa, B. G. Malmström and L. G. Lundberg, *FEBS Lett.*, 1989, **253**, 99–102.
- 23 B. L. Vallee and R. J. Williams, *Proc. Natl. Acad. Sci.*, 1968, **59**, 498–505.
- 24 B. G. Malmström, *Eur. J. Biochem.*, 1994, **223**, 711–718.
- 25 J. R. Winkler, P. Wittung-Stafshede, J. Leckner, B. G. Malmström and H. B. Gray, *Proc. Natl. Acad. Sci.*, 1997, **94**, 4246 LP – 4249.
- 26 R. A. Marcus and N. Sutin, *Biochim. Biophys. Acta - Rev. Bioenerg.*, 1985, **811**, 265–322.
- 27 U. Ryde, M. H. M. Olsson, B. O. Roos, J. O. A. De Kerpel and K. Pierloot, *JBIC J. Biol. Inorg. Chem.*, 2000, **5**, 565–574.
- 28 H. A. Jahn, E. Teller and F. G. Donnan, *Proc. R. Soc. London. Ser. A - Math. Phys. Sci.*, 1937, **161**, 220–235.
- 29 D. W. Randall, D. R. Gamelin, L. B. LaCroix and E. I. Solomon, *JBIC J. Biol. Inorg. Chem.*, 2000, **5**, 16–29.
- 30 R. H. Holm, P. Kennepohl and E. I. Solomon, *Chem. Rev.*, 1996, **96**, 2239–2314.
- 31 E. I. Solomon, K. W. Penfield, A. A. Gewirth, M. D. Lowery, S. E. Shadle, J. A. Guckert and L. B. LaCroix, *Inorganica Chim. Acta*, 1996, **243**, 67–78.
- 32 L. B. LaCroix, D. W. Randall, A. M. Nersissian, C. W. G. Hoitink, G. W. Canters, J. S. Valentine and E. I. Solomon, *J. Am. Chem. Soc.*, 1998, **120**, 9621–9631.
- 33 S. E. Shadle, J. E. Penner-Hahn, H. J. Schugar, B. Hedman, K. O. Hodgson and E. I. Solomon, *J. Am. Chem. Soc.*, 1993, **115**, 767–776.
- 34 A. A. Gewirth and E. I. Solomon, *J. Am. Chem. Soc.*, 1988, **110**, 3811–3819.
- 35 K. W. Penfield, A. A. Gewirth and E. I. Solomon, *J. Am. Chem. Soc.*, 1985, **107**, 4519–4529.
- 36 S. Larsson, A. Broo and L. Sjoelin, *J. Phys. Chem.*, 1995, **99**, 4860–4865.
- 37 P. Wittung-Stafshede, M. G. Hill, E. Gomez, A. J. Di Bilio, B. G. Karlsson, J. Leckner, J. R. Winkler, H. B. Gray and B. G. Malmström, *JBIC J. Biol. Inorg. Chem.*, 1998, **3**, 367–370.
- 38 A. S. Brill, *Biophys. Chem.*, 1999, **80**, 129–138.
- 39 S. Ghosh, X. Xie, A. Dey, Y. Sun, C. P. Scholes and E. I. Solomon, *Proc. Natl. Acad. Sci.*, 2009, **106**, 4969–4974.
- 40 W. R. Hagen, *Metallomics*, 2019, **11**, 1768–1778.
- 41 J. Stanek, A. Hoffmann and S. Herres-Pawlis, *Coord. Chem. Rev.*, 2018, **365**, 103–121.
- 42 C. A. Hurd, N. A. Besley and D. Robinson, *J. Comput. Chem.*, 2017, **38**, 1431–1437.
- 43 N. J. Fowler, C. F. Blanford, J. Warwicker and S. P. de Visser, *Chem. – A Eur. J.*, 2017, **23**, 15436–15445.
- 44 D. Bím and A. N. Alexandrova, [10.26434/chemrxiv.13615853.v1](https://doi.org/10.26434/chemrxiv.13615853.v1), , DOI:10.26434/chemrxiv.13615853.v1.
- 45 D. Shirvanyants, A. N. Alexandrova and N. V. Dokholyan, *Bioinformatics*, 2011, **27**, 1327–1329.
- 46 J. Szuster, U. A. Zitare, M. A. Castro, A. J. Leguto, M. N. Morgada, A. J. Vila and D. H. Murgida, *Chem. Sci.*, 2020, **11**, 6193–6201.
- 47 G. S. Kachalova, A. C. Shosheva, G. P. Bourenkov, A. A. Donchev, M. I. Dimitrov and H. D. Bartunik, *J. Inorg. Biochem.*, 2012, **115**, 174–181.
- 48 R. G. Hadt, N. Sun, N. M. Marshall, K. O. Hodgson, B. Hedman, Y. Lu and E. I. Solomon, *J. Am. Chem. Soc.*, 2012, **134**, 16701–16716.
- 49 N. M. Marshall, D. K. Garner, T. D. Wilson, Y. G. Gao, H. Robinson, M. J. Nilges and Y. Lu, *Nature*, 2009, **462**, 113–116.
- 50 L. Yang, D. R. Powell and R. P. Houser, *Dalt. Trans.*, 2007, 955–964.